

A New Basis for Sparse Principal Component Analysis

Fan Chen

Department of Statistics, University of Wisconsin–Madison
and

Karl Rohe*

Department of Statistics, University of Wisconsin–Madison

September 8, 2021

Abstract

Previous versions of sparse principal component analysis (PCA) have presumed that the eigen-basis (a $p \times k$ matrix) is approximately sparse. We propose a method that presumes the $p \times k$ matrix becomes approximately sparse after a $k \times k$ rotation. The simplest version of the algorithm initializes with the leading k principal components. Then, the principal components are rotated with an $k \times k$ orthogonal rotation to make them approximately sparse. Finally, soft-thresholding is applied to the rotated principal components. This approach differs from prior approaches because it uses an orthogonal rotation to approximate a sparse basis. One consequence is that a sparse component need not to be a leading eigenvector, but rather a mixture of them. In this way, we propose a new (rotated) basis for sparse PCA. In addition, our approach avoids “deflation” and multiple tuning parameters required for that. Our sparse PCA framework is versatile; for example, it extends naturally to a two-way analysis of a data matrix for simultaneous dimensionality reduction of rows and columns. We provide evidence showing that for the same level of sparsity, the proposed sparse PCA method is more stable and can explain more variance compared to alternative methods. Through three applications—sparse coding of images, analysis of transcriptome sequencing data, and large-scale clustering of social networks, we demonstrate the modern usefulness of sparse PCA in exploring multivariate data.

Keywords: Column sparsity, dimensionality reduction, orthogonal rotation, sparse matrix decomposition, independent component analysis

*The authors gratefully acknowledge National Science Foundation grant DMS-1612456 and DMS-1916378 and Army Research Office grant W911NF-15-1-0423.

1 Introduction

Principal component analysis (PCA), introduced in the early 20th century [Pearson, 1901, Hotelling, 1933], is one of the most prevalent tools in exploratory multivariate data analysis. PCA projects higher-dimensional data into a lower-dimensional space that is spanned by some uncorrelated principal components (PCs), with the vast majority of the variance in the data kept. It is, however, commonly conceived that PCs are difficult to interpret [e.g., Jeffers, 1967], as each PC is a linear combination of many, if not all, original variables. To remedy such disadvantage, sparse PCA estimates “sparse” PCs, each of which consists of a small subset of original variables [Zou and Xue, 2018].

Sparse PCA is originally formulated as an optimization problem over the loading coefficients with a cardinality constraint. Such non-convex constraint results in an NP-hard problem in the strong sense [Tillmann and Pfetsch, 2014]. In order to circumvent the obstacle, various methods have been proposed, such as the iconic regression-based approach by Zou et al. [2006], a convex relaxation to semidefinite programming [d’Aspremont et al., 2007], the penalized matrix decomposition framework of Witten et al. [2009], and the generalized power method due to Journée et al. [2010]. More recently, theoretical developments of sparse PCA have covered the consistency [Johnstone and Lu, 2009, Shen et al., 2013], variable selection properties [Amini and Wainwright, 2009], rates of convergence, the minimaxity over some Gaussian or sub-Gaussian classes [Vu and Lei, 2013, Cai et al., 2013], and the statistical-computational trade-offs under the restricted covariance concentration condition [Berthet and Rigollet, 2013, Wang et al., 2016].

Despite the extensive literature of sparse PCA, there are two enigmas. First, sparse PCA often explains far less variance in the data than PCA does (Figure 1). While this may appear to be a trade-off for sparsity, our results show that a substantial improvement is possible. Second, the most common formulations of sparse PCA only estimate a single component at a time and thus rely on a matrix deflation after estimating each component. This deflation entails complications of multiple tuning parameters, non-orthogonality, and

By allowing for a rotated basis, sparse PCA can explain nearly as much variance as PCA

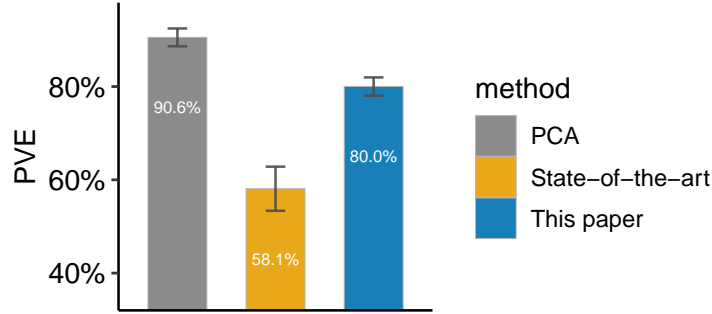


Figure 1: Comparison of the explanatory power of sparse PCA methods. Each bar shows the proportion of variance explained (PVE) by 16 PCs. For two sparse PCA methods, an error bar (based on the three-sigma rule) depicts the variation of PVE over 30 replicates. More details about the simulated data and settings (e.g., sparsity constraints) are described in Section 4.1.

sub-optimality [Mackey, 2008]. Identifiability and consistency present more subtle issues; there is no reason to assume a priori distinct eigenvalues or that the gaps between the eigenvalues are small [Vu et al., 2013]. Estimating the subspace spanned by multiple sparse PCs at once overcomes this dilemma [Vu et al., 2013].

There are two distinct notions of subspace sparsity: row sparsity and column sparsity [Vu and Lei, 2013]. Contemporary approaches to sparse PCA primarily focus on row sparsity, which implies that the eigenvectors of the covariance matrix themselves are sparse [e.g., Moghaddam et al., 2006]. The second notion, column sparsity, is an alternative. A column sparse subspace *“is one which has some orthogonal basis consisting of sparse vectors. This means that the choice of basis is crucial; the existence of a sparse basis is an implicit assumption behind the frequent use of rotation techniques by practitioners to help interpret principal components”* [Vu and Lei, 2013]. Row sparsity is the most prevalent notion of sparsity used in contemporary sparse PCA, yet it does not appear to describe many contemporary parametric multivariate models; conversely, many contemporary parametric models in multivariate statistics can be estimated with the sparse PCA approaches that can identify column sparsity [Rohe and Zeng, 2020].

In high-dimensional regression, sparse penalties such as the Lasso resolve an invariance; there is an entire space of solutions b which exactly interpolate the data $Y = Xb$ and presuming that the solution b is sparse can make the solution unique. Interestingly, there is no analogue to “sparsity resolving an invariance” for the estimation of row sparse subspace, but there is a very clear analogue in estimating column sparse subspace; the basis is determined by the one that provides the most sparse representation of data.

1.1 Our contributions

In this work, we propose a new method, sparse component analysis (SCA), to estimate multiple PCs that are column sparse. The column sparsity is achieved by allowing an orthogonal rotation to PCs prior to imposing any sparsity constraints. The algorithm is motivated by two facts. First, an orthogonal rotation does not affect the total variance explained by a given set of PCs. Second, by choosing the orthogonal rotation carefully, PCs can be aligned closely with the coordinate axes, making them approximately sparse (Figure 2). This technique has been commonly adapted in factor analysis, a close cousin of PCA [Thurstone, 1931, Kaiser, 1960, Jolliffe, 1995]. For example, the varimax rotation [Kaiser, 1958] is a popular choice in the psychology literature. SCA incorporates the orthogonal rotation and sparsity constraints to find the sparse and orthogonal basis in a subspace (i.e., column sparse PCs). We show in Proposition 1 that

column sparse PCs can explain more variance in the data than row sparse PCs.

We validated this with numerical experiments. Additionally, the simulations suggest that SCA is more stable and robust across tuning parameters than existing sparse PCA methods. Our framework of SCA generalizes naturally to a two-way analysis of a data matrix for simultaneous row and column dimensionality reductions. For this, we introduce a low-rank matrix approximation method called sparse matrix approximation (SMA). The SMA builds on the penalized matrix decomposition previously proposed by Witten et al. [2009]. Furthermore, the SMA provides a unified view of sparse PCA and other modern multi-

The same data in seven dimensions, before and after rotation. After the sparse rotation, each PC uses only a small subset of the original variables.

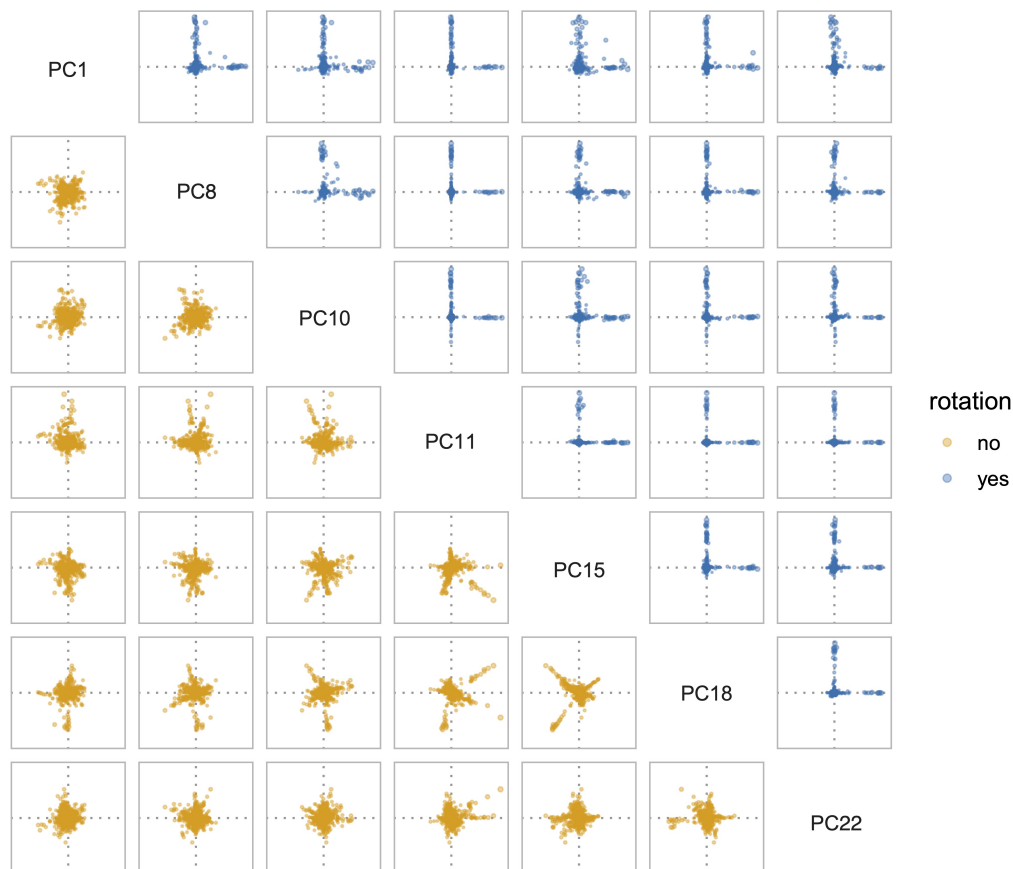


Figure 2: Loadings of seven principal components (PCs) from a large scale social network matrix. Each (off-diagonal) panel shows the loadings of two PCs on the original variables (displayed as points). The lower-triangular panels (yellow) depict the PCs before a rotation. The upper-triangular panels (blue) display the PCs after an orthogonal rotation. The PCs before and after the rotation have no special or corresponding relationship. In each panel, two perpendicular dotted lines (grey) indicate the coordinate axes. See Section 5.3 for details about the data analyzed.

variate data analysis, including sparse independent component analysis [see, e.g., [Comon, 1994](#)]. Finally, we demonstrate our sparse PCA methods with various high-dimensional data applications, including sparse coding of images, blind source separation, analysis of single-cell transcriptome data, and large-scale clustering of social networks. We find compelling evidence for the usefulness of our approach, despite concerns about the consistency of PCA in high-dimensions.

1.2 Organization

The rest of this paper goes as follows. Section 2 describes the methods. Section 3 compares SCA to existing methods. Section 4 compares different sparse PCA methods using simulated data. Section 5 applies SCA to several high-dimensional datasets. Section 6 concludes the paper with some discussions.

1.3 Notations

In this paper, we discuss the *entrywise* matrix norm only. For any matrix $A \in \mathbb{R}^{m \times n}$, its entrywise ℓ_p -norm is defined as $\|A\|_{p,p} = (\sum_{i=1}^m \sum_{j=1}^n |A_{ij}|^p)^{1/p}$. For simplicity, we also use the notation $\|A\|_p$ for entrywise norm, rather than the norm induced by a vector norm. In particular, the Frobenius norm (or the Hilbert-Schmidt norm) is then an alias of entrywise ℓ_2 -norm, $\|A\|_F = \sqrt{\sum_{i=1}^m \sum_{j=1}^n A_{ij}^2} = \|A\|_2$. Throughout, the following sets of matrices are frequently considered. $\mathcal{U}(n) = \{U \in \mathbb{R}^{n \times n} \mid U^T U = U U^T = I_n\}$ denotes all orthogonal (unitary) matrices in \mathbb{R}^n . $\mathcal{V}(n, k) = \{V \in \mathbb{R}^{n \times k} \mid V^T V = I_k\}$ represents the Stiefel manifold in \mathbb{R}^n , and $\mathcal{B}(n, k) = \{V \in \mathbb{R}^{n \times k} \mid V^T V \preceq I_k\}$ is its convex hull [[Gallivan and Absil, 2010](#)].

2 The methods

Consider the data matrix $X \in \mathbb{R}^{n \times p}$ of n observations (or samples) on p variables. Without loss of generality, we assume that each column of X is centered (i.e. mean-zero) unless

otherwise noted. PCA finds some (say k) uncorrelated linear transformations of the original variables such that after the linear transformations, the most variance is kept. That is,

$$\underset{Y}{\text{maximize}} \quad \|XY\|_F \quad \text{subject to } Y \in \mathcal{V}(p, k), \quad (1)$$

where the feasible set is the Stiefel manifold, $\mathcal{V}(p, k) = \{Y \in \mathbb{R}^{p \times k} \mid Y^T Y = I_k\}$. The j th PC is the linear combination of original variables whose coefficients are in the j th columns of Y . The coefficients are often called *loadings* (or loading coefficients). Note that loadings are usually non-zero (i.e., Y is usually not sparse). The transformed data $S = XY \in \mathbb{R}^{n \times k}$ contains the *scores*. That is, S_{ij} is the score of the i th sample on the j th PC.

In PCA, PCs are often defined sequentially. That is, in order to find the k th PCs, we fix the previous $k - 1$ PCs and solve (1); repeat this for $k = 1, 2, \dots$ in order. Such definition ensures the first k PCs together always explain the most variance in the data. By contrast, for sparse PCA, we reason in the following that it is sufficient to solve the optimization problem for all PCs at once. Note first that the solution to (1) is a subspace, because if Y^* is an optimizer of (1), then for any orthogonal matrix $R \in \mathcal{U}(k)$, $Y^* R$ is also an optimizer. The solution to (1) being a rotation-invariant subspace is desirable because it allows a sparsity-enabling orthogonal rotation to any given solution. Importantly, such rotation exists under the assumption of *column sparsity* [see Section 2.1.1 and [Vu and Lei, 2013](#)]. We thereby propose a new method for sparse PCA.

2.1 Sparse component analysis

For sparse PCA, we impose an ℓ_1 -norm constraint¹ on the loadings and formulate the following minimization of matrix reconstruction error:

$$\begin{aligned} & \underset{Z, B, Y}{\text{minimize}} && \|X - ZBY^T\|_F \\ & \text{subject to} && Z \in \mathcal{V}(n, k), Y \in \mathcal{V}(p, k), \|Y\|_1 \leq \gamma, \end{aligned} \quad (2)$$

¹The ℓ_1 -norm constraint could be replaced by other sparsity constraints, e.g., the ℓ_0 -norm analogue.

where $\gamma > 0$ is the sparsity controlling parameter, and the columns of Y are PC loadings. ZBY^T is an approximation of X .

The fundamental difference between formulation (2) and previous sparse PCA formulations is that the middle B matrix is not necessarily diagonal. Compared to the diagonal B case, this added flexibility has two merits—(i) it allows PCs to be column sparse and (ii) it allows sparse PCs to explain more variance in the data.

2.1.1 Column sparsity

Our formulation (2) presumes the PCs are column sparse. That is, given the subspace of PCs, there exists a orthogonal rotation, such that after the rotation, the PCs are approximately sparse.

Let UDV^T be the low-rank singular value decomposition (SVD) of X , where $U \in \mathcal{V}(n, k)$ and $V \in \mathcal{V}(p, k)$ contain singular vectors, and $D \in \mathbb{R}^{k \times k}$ is a diagonal matrix with the diagonal entries in decreasing order, and $k \leq \min\{n, p\}$ is the rank. For any two orthogonal matrices $O, R \in \mathcal{U}(k)$, define $Z = UO$, $B = O^TDR$, and $Y = VR$. With these definitions,

$$X \approx UDV^T = (UO)(O^TDR)(VR)^T = ZBY^T.$$

As such, ZBY^T approximates X as well as UDV^T . In particular, the middle B matrix is not diagonal because it absorbs the orthogonal matrices (O and R). Z and Y are orthogonally rotated from U and V , and both matrices still have orthogonal columns. Hence, by imposing an ℓ_1 -norm constraint on Y to make it approximately sparse, we presume that there exists at least one orthogonal basis for the column space of V (i.e., the eigenvectors' subspace), which is not necessarily the original coordinate basis, such that the PCs are sparse under that basis.

Remark 1. *The formulation of SCA does not implicitly order sparse PCs. This is because permuting the columns of Y , which can be absorbed by the orthogonal matrix R , does not change the approximation of ZBY^T . As such, the solution to (2) is not unique. In practice*

(see Section 4.1), we sort sparse PCs by the explained variance (EV) of individual PCs, which is defined as $\|Xy\|_2^2$, where $y \in \mathbb{R}^p$ contains the loadings of a PC.

2.1.2 Explained variance in the data

A non-diagonal middle B matrix facilitates the more general formulation of column sparse PCA. Specially, if B is restricted to diagonal, the formulation reduces to row sparse PCA.² Row sparse PCA presumes that given the subspace of PCs (i.e., the subspace spanned by some singular vectors of X), the PC loadings are approximately sparse by themselves (i.e., the singular vectors align closely with the natural coordinate axes). The next proposition compares column and row sparse PCA in terms of the matrix reconstruction error (the proof is provided in Appendix A).

Proposition 1 (Comparison of row and column sparsity). *Let $X \in \mathbb{R}^{n \times p}$ be any matrix. Suppose $S_Z \subseteq \mathbb{R}^{n \times k}$ and $S_Y \subseteq \mathbb{R}^{p \times k}$ are the feasible sets for Z and Y respectively, where $k \leq \min(n, p)$. Then, subject to $Z \in S_Z$, $Y \in S_Y$, and D is diagonal, it holds that*

$$\min_{Z, B, Y} \|X - ZBY^T\|_F \leq \min_{Z, D, Y} \|X - ZDY^T\|_F.$$

Proposition 1 says that the solution to column sparse PCA has smaller reconstruction error of the data matrix than row sparse PCA. Since the squared matrix reconstruction error here is the unexplained variance in the data, it follows that the solution to column sparse PCA can capture more variance in the data than row sparse PCA.

Remark 2. *From a parametric perspective, SCA explains more variance because it uses $k^2 - k$ more parameters in the B matrix. Relative to the total number of parameters, this is typically a small increase; the Z and Y matrices contain roughly $(n + p)k$ parameters, and typically k is much smaller than $n + p$. Whether these additional parameters in B are statistically justified must be addressed in a case-by-case basis. In our limited experience*

²This restricted formulation is essentially a low-rank SVD with an additional sparsity constraint on the right singular vectors.

with these techniques, the additional parameters are easily justified because the proportion of variance explained dramatically increases (see Section 4.1); the output becomes more stable across initializations, perturbations, and tuning parameters (see Section 4.2); and the estimated factors are easily interpretable (see Section 5.2 and 5.3).

2.2 An algorithm for SCA

To solve SCA, the following lemma translates (2) into an equivalent and more convenient form (the proof can be found in Appendix A).

Lemma 1 (Bilinear form of SCA). *Solving the minimization in (2) is equivalent to solving the following maximization problem,*

$$\underset{Z, Y}{\text{maximize}} \quad \|Z^T X Y\|_F \quad \text{subject to } Z \in \mathcal{V}(n, k), Y \in \mathcal{V}(p, k), \|Y\|_1 \leq \gamma. \quad (3)$$

In particular, for the optimizer in (2), $B = Z^T X Y$.

Due to the non-convexity of ℓ_2 -equality constraints ($Z \in \mathcal{V}(n, k)$ and $Y \in \mathcal{V}(p, k)$), the feasible set in (3) is not convex in general. We replace the feasible set with its convex hull using some ℓ_2 -inequality constraints for simplicity,

$$\underset{Z, Y}{\text{maximize}} \quad \|Z^T X Y\|_F \quad \text{subject to } Z \in \mathcal{B}(n, k), Y \in \mathcal{B}(p, k), \|Y\|_1 \leq \gamma. \quad (4)$$

Due to the Karush-Kuhn-Tucker conditions [see, e.g., Nocedal and Wright, 2006], one could expect the solution to fall on the boundary (i.e., $Z \in \mathcal{V}(n, k)$, $Y \in \mathcal{V}(p, k)$, and $\|Y\|_1 = \gamma$) so long as the sparsity parameters are chosen such that $k \leq \gamma \leq k\sqrt{p}$.³ As such, local optima are not necessarily global optima. We discuss a data-driven method of tuning the sparsity parameters in Supplementary Section B.

Next, we describe an algorithm that computes sparse PCs as formulated in (4). The input includes a data matrix X , the desired number of sparse PCs k , and optionally the

³This is for the set $\{Y \in \mathbb{R}^{p \times k} \mid \|Y\|_1 = \gamma\}$ to intersect with the Stiefel manifold $\mathcal{V}(p, k)$.

sparsity controlling parameters γ . In our experiences, a default value of $\gamma = \sqrt{pk}$ appears to generate robust and interpretable sparse PCs (see, e.g., Section 4.2). The algorithm outputs the loadings of k sparse PCs. The SCA algorithm initializes $Z \in \mathcal{V}(n, k)$ and $Y \in \mathcal{V}(p, k)$ with the top k left and right singular vectors of X respectively. Once initialized, the algorithm alternatively updates Z and Y ; fixing one and optimizing the other until convergence. The iteration is because the objective function is bilinear in Z and Y , allowing for fast updates. Specifically, with Y fixed, (4) takes the form

$$\underset{Z}{\text{maximize}} \quad \|Z^T XY\|_{\text{F}} \quad \text{subject to } Z \in \mathcal{B}(n, k). \quad (5)$$

With Z fixed, (4) takes the form

$$\underset{Y}{\text{maximize}} \quad \|Z^T XY\|_{\text{F}} \quad \text{subject to } Y \in \mathcal{B}(p, k), \|Y\|_1 \leq \gamma. \quad (6)$$

2.2.1 Update Z fixing Y

The update of Z fixing Y in (5) is algebraic. The following lemma provides a set of solutions to (5), which is extended from Theorem 7.3.2 in Horn and Johnson [1985] (the proof is included in Appendix A for completeness).

Lemma 2 (Maximization without sparsity constraint). *Given a full-rank matrix $X \in \mathbb{R}^{n \times p}$, with $p \leq n$, let the singular values of X be σ_i for $i = 1, 2, \dots, p$. Then,*

$$\max_{Y \in \mathcal{V}(n, p)} \|X^T Y\|_{\text{F}} = \sum_{i=1}^p \sigma_i$$

with the maximizer $Y^ = \text{polar}(X)$, up to any orthogonal rotation from the right. Here, $\text{polar}(X) = X(X^T X)^{-1/2}$ is the polar of X .*

Due to Lemma 2, the SCA algorithm updates Z with the polar of XY , $\hat{Z} = \text{polar}(XY)$, which can be computed in $\mathcal{O}(nk)$ time [Journée et al., 2010].

2.2.2 Update Y fixing Z

To update Y fixing Z , we start by solving the non-sparse version of (6) (i.e., remove the sparsity constraint $\|Y\|_1 \leq \gamma$),

$$\underset{Y}{\text{maximize}} \quad \|Z^T XY\|_F \quad \text{subject to } Y \in \mathcal{B}(p, k). \quad (7)$$

Let $\tilde{Y} = \text{polar}(X^T Z)$. Then, \tilde{Y} is one element in the subspace of the solutions to (7). Before imposing the sparsity constraint, we look for an orthogonal rotation R to \tilde{Y} to minimize $\|\tilde{Y}R\|_1$. However, $\|Y\|_1$ is not a smooth function of Y if it contains at least one zero entry, entailing the complications of defining sub-gradients. Alternatively, the SCA algorithm minimizes a smoother criterion based on the $\ell_{4/3}$ norm:

$$\underset{R}{\text{minimize}} \quad \|\tilde{Y}R\|_{\frac{4}{3}} \quad \text{subject to } R \in \mathcal{U}(k). \quad (8)$$

This sub-problem leads to the varimax rotation (see Section 2.2.3) that is widely applied in factor analysis [Kaiser, 1958]. We denote $Y^* = \tilde{Y}R^*$ to be the orthogonally rotated solution to (7), where R^* is the solution to (8). Finally, considering the ℓ_1 -norm sparsity constraint, we apply the element-wise soft-thresholding of Y^* with the sparsity parameter γ , which is defined as [Donoho, 1995, Tibshirani, 1996]

$$[T_\gamma(Y^*)]_{ij} = \text{sign}(Y_{ij}^*) \cdot (|Y_{ij}^*| - t)_+, \quad (9)$$

where $t > 0$ is the threshold determined by the equation $\|T_\gamma(Y^*)\|_1 = \gamma$, and x_+ equals x if $x > 0$ or 0 otherwise. We discuss several properties of soft-thresholding in Supplementary Section C. In summary, the update of Y given Z consists of three steps that we call ‘‘Polar-Rotate-Shrink’’ (PRS, Algorithm 1)—first, compute a solution to the unconstrained problem (7); second, rotate with varimax; third, soft-threshold all of the elements. Algorithm 2 summarizes the algorithm of SCA.

<p>Input: $A \in \mathbb{R}^{p \times k}$, sparsity parameter γ (optional, default to \sqrt{pk})</p> <p>Procedure PRS(A):</p> <p> $\tilde{Y} \leftarrow$ left singular vectors of A</p> <p> $Y^* \leftarrow$ rotate \tilde{Y} with varimax // Section 2.2.3</p> <p> $\hat{Y} \leftarrow$ soft-threshold Y^* with parameter γ</p> <p>Output: \hat{Y}</p>

Algorithm 1: Polar-Rotate-Shrink (PRS)

<p>Input: Data matrix X and a number of components k</p> <p>Procedure SCA(X, k):</p> <p> Initialize \hat{Z} and \hat{Y} with the top k left and right singular vectors of X</p> <p> repeat</p> <p> $\hat{Y} \leftarrow$ PRS($X^T \hat{Z}$) // Algorithm 1</p> <p> $\hat{Z} \leftarrow$ polar($X \hat{Y}$) // Lemma 2</p> <p> until <i>convergence</i></p> <p>Output: Sparse loadings \hat{Y}</p>
--

Algorithm 2: Sparse Component Analysis (SCA)

2.2.3 The varimax rotation

For any matrix $A \in \mathbb{R}^{p \times k}$, the *varimax criterion* is defined as the sum of column (sample) variance of squared elements (A_{ij}^2) [Kaiser, 1958]:

$$C_{\text{varimax}}(A) = \sum_{j=1}^k \left[\frac{1}{p} \sum_{i=1}^p A_{ij}^4 - \frac{1}{p^2} \left(\sum_{i=1}^p A_{ij}^2 \right)^2 \right].$$

For a fixed matrix $Y \in \mathbb{R}^{p \times k}$, the *varimax rotation* seeks an orthogonal rotation $R \in \mathbb{R}^{k \times k}$ to maximize the varimax criterion evaluated at YR ,

$$\underset{R}{\text{maximize}} \quad C_{\text{varimax}}(YR) \quad \text{subject to } R \in \mathcal{U}(k). \tag{10}$$

It is commonly used in factor analysis for producing nearly sparse and interpretable loadings of PCs, especially in the psychology literature. The varimax rotation is easy to compute;

for example, the base function `varimax` in `R` implements a gradient projection algorithm of it [Bernaards and Jennrich, 2005]. Jennrich [2001] showed that the gradient projection algorithm converges to a local optimum from any starting point and enjoys geometric (or linear) convergence rate.

The varimax criterion naturally links to the $\ell_{4/3}$ -norm objective function in (8). Since $Y \in \mathcal{V}(p, k)$, the columns of Y have unit length. Hence, $\sum_{i=1}^p Y_{ij}^2 = 1$, and the varimax criterion reduces to a simpler form (also known as the *quartimax* criterion as introduced by Carroll [1953]) up to an additive constant:

$$C_{\text{quartimax}}(Y) = \sum_{i=1}^p \sum_{j=1}^k Y_{ij}^4 = \|Y\|_4^4,$$

which is the ℓ_4 -norm of Y to the power of 4. Next, by the Hölder’s inequality (using the Hölder conjugates $4/3$ and 4) and the power mean inequality (and that $\|Y\|_F = \sqrt{k}$),

$$\|Y\|_{\frac{4}{3}} \|Y\|_4 \geq \|Y\|_1 \geq \|Y\|_F = \sqrt{k}.$$

This implies that maximizing the varimax criterion is the dual problem of minimizing the $\ell_{4/3}$ -norm objective. Hence, to update Y in the algorithm of SCA, we invoke the varimax rotation in (10) as a proxy of (8).

Remark 3. Besides *varimax*, we experimented the orthogonal rotation that directly minimizes the ℓ_1 norm, which we call the “*absmin*” rotation:

$$\underset{R}{\text{minimize}} \quad \|YR\|_1 \quad \text{subject to } R \in \mathcal{U}(k). \quad (11)$$

However, the objective function is not smooth at those R where YR contains at least one zero element; this posts challenges to solving (11). For example, we tried a gradient projection algorithm using the gradient direction $Y^T \text{sign}(YR)$, where $\text{sign}(\cdot)$ is the element-wise sign function, yet the algorithm hardly converges. It is worth noting that in our lim-

ited experiments, where we used the *absmin* rotation but only allowed fifteen iterations of this gradient projection algorithm, we obtained marginally better solutions, in terms of explained variance, than using the *varimax* rotation (see Section 4.1). It is of future interest to investigate alternative orthogonal rotations that are easy to compute and can generate approximately sparse structure.

2.3 Sparse matrix approximation

In the SCA algorithm above, a sparsity constraint can also be applied to Z , in addition to Y . We call this sparse matrix approximation (SMA). We define SMA as the solution to a matrix reconstruction error minimization problem:

$$\begin{aligned} & \underset{Z, B, Y}{\text{minimize}} && \|X - ZBY^T\|_F && (12) \\ & \text{subject to} && Z \in \mathcal{B}(n, k), \mathcal{P}_1(Z) \leq \gamma_z, \\ & && Y \in \mathcal{B}(p, k), \mathcal{P}_2(Y) \leq \gamma_y, \end{aligned}$$

where $\gamma_z > 0$ and $\gamma_y > 0$ are the sparsity controlling parameters, and \mathcal{P}_1 and \mathcal{P}_2 are some *penalty* functions that promote sparsity. If γ_z is so large that $\mathcal{P}_1(Z) \leq \gamma_z$ is always satisfied, then (12) is equivalent to SCA. Similar to Lemma 1, we transform (12) into an equivalent and more convenient form (the proof is almost identical to that of Lemma 1 thus is omitted),

$$\begin{aligned} & \underset{Z, Y}{\text{maximize}} && \|Z^T XY\|_F && (13) \\ & \text{subject to} && Z \in \mathcal{B}(n, k), \mathcal{P}_1(Z) \leq \gamma_z, \\ & && Y \in \mathcal{B}(p, k), \mathcal{P}_2(Y) \leq \gamma_y. \end{aligned}$$

The two criteria in (12) and (13) are equivalent if and only if $B = Z^T XY$. We interpret B as the “*score*” of SMA, since the solution to (12) maximizes the sum of squares of its elements, $\sum_{i,j} B_{ij}^2$. It is also worth noting that the squared matrix reconstruction error

equals to $\|X\|_F^2 - \|B\|_F^2$ (see the proof of Lemma 1).

Since SMA is a simple extension from SCA, we extend Algorithm 2 for SMA in Algorithm 3, where we apply PRS to Z in addition to Y . The output includes the estimated Z , B , and Y .

Input: data matrix $X \in \mathbb{R}^{n \times p}$ and the approximation rank k
Procedure SMA (X, k):
Initialize \hat{Z} and \hat{Y} with the top k left and right singular vectors of X
repeat
 $\hat{Z} \leftarrow \text{PRS}(X\hat{Y})$ // Algorithm 1
 $\hat{Y} \leftarrow \text{PRS}(X^T\hat{Z})$ // Algorithm 1
until *convergence*
 $\hat{B} \leftarrow \hat{Z}^T X \hat{Y}$
Output: \hat{Z} , \hat{B} , and \hat{Y}

Algorithm 3: Sparse Matrix Approximation (SMA) with $\mathcal{P}_1(A) = \mathcal{P}_2(A) = \|A\|_1$.

We highlight that SMA generalizes the popular penalized matrix decomposition (PMD) proposed by Witten et al. [2009], which is also similar to the method of Shen and Huang [2008]. The PMD also approximates a data matrix $X \in \mathbb{R}^{n \times p}$ by the product of three matrices, ZDY^T , where $Z \in \mathcal{V}(n, k)$ and $Y \in \mathcal{V}(p, k)$ are presumed sparse, and $D \in \mathbb{R}^{k \times k}$ is a diagonal matrix whose diagonal entries are in decreasing order, and k is the rank of the matrix approximation. For sparsity, PMD applies penalty functions to Z and Y , leading to the matrix reconstruction error minimization formulation of PMD:⁴

$$\begin{aligned} & \underset{U, D, V}{\text{minimize}} && \|X - ZDY^T\|_F \\ & \text{subject to} && Z \in \mathcal{B}(n, k), \mathcal{P}_1(Z) \leq \gamma_z, \\ & && Y \in \mathcal{B}(p, k), \mathcal{P}_2(Y) \leq \gamma_y, \\ & && D \text{ is diagonal,} \end{aligned}$$

where $\gamma_z, \gamma_y > 0$ are parameters that control the sparsity of Z and Y , and \mathcal{P}_1 and \mathcal{P}_2 are

⁴The paper originally considers the PMD with $k = 1$. The PMD finds multiple factors sequentially using a deflation technique.

some convex penalty function (e.g. ℓ_1 -norm).

The single difference between SMA and PMD is the the diagonal constraint on the middle matrix. In this way, SMA generalizes PMD, because, SMA estimates $k^2 - k$ more parameters in B than PMD (see Remark 2). Proposition 1 suggests that the reconstruction error of SMA is less or equal to that of PMD (see also Remark 4 in Appendix A). Algorithmically, in order to compute PMD, Witten et al. [2009] proposed to find the solution by sequentially maximizing B_{ii} for $i = 1, 2, \dots, k$ (recall that $B = Z^TXY$). By contrast, solving the SMA in (13) amounts to maximizing the entirety of the score matrix, that is, $\|B\|_F$.

3 Connections to existing methods

In this section, we compare SCA with several existing methods of sparse PCA and discuss two variants and one extension of SCA.

3.1 Existing sparse PCA methods

The formulation of SCA is akin to multiple existing sparse PCA formulations. However, the possibility of orthogonal rotations has not been explored thoroughly, despite the plethora of available methods. In this section, we elucidate these connections and point to some differences.

SPCA [Zou et al., 2006] SPCA is motivated to maximize the explained variance in the data [Jolliffe et al., 2003]. The formulation of SPCA minimizes a “residual sum of squares plus penalties” type of criterion,

$$\underset{U, V}{\text{minimize}} \quad \|X - XVU^T\|_F^2 + \lambda_1\|V\|_F^2 + \lambda_2\|V\|_1 \quad \text{subject to } U \in \mathcal{V}(p, k),$$

where $V \in \mathbb{R}^{p \times k}$ is the sparse loadings of interest, and λ_1 and λ_2 are tuning parameters. We note that the first term in the objective function is also invariant to any or-

thogonal rotation applied to U and V , because $\|X - XVU^T\|^2 = \|X - X(VR)(UR)^T\|^2$ for any $R \in \mathcal{U}(k)$. However, the algorithm of SPCA for U and V does not use orthogonal rotations to search over the solution space, as it is adapted from the elastic net [Zou and Hastie, 2005]. Explicitly searching for a sparsity-enabling rotation R could help to find a smaller objective value in SPCA.

SPC [Witten et al., 2009] SPC finds one sparse PC at a time,

$$\underset{u,v}{\text{maximize}} \quad u_i^T X v_i \quad \text{subject to} \quad \|u_i\|_2 = 1, \|v_i\|_2 = 1, \|v_i\|_1 \leq \gamma, \quad (14)$$

where $v_i \in \mathbb{R}^p$ contains the loadings of the i th sparse PC, for $1 \leq i \leq k$. When $k = 1$, our formulation of SCA in (3) takes the same form as the SPC formulation, where an orthogonal rotation is unnecessary. When $k > 1$, however, SPC searches for sparse PCs sequentially and does not rotate PCs, unlike SCA, which computes k sparse PCs simultaneously. SPC is similar to the rSVD proposed by Shen and Huang [2008] and the TPower proposed by Yuan and Zhang [2013] in that all the three methods rely on a deflation technique for multiple PCs. This technique entails complications of, for example, non-orthogonality and sub-optimality [Mackey, 2008]. More generally, these methods can each be viewed as a special case of the following GPower formulation.

GPower [Journée et al., 2010] GPower has a “block version” that computes multiple sparse PCs simultaneously by considering a linear combination of individual sparse PCA (as formulated in SPC),

$$\underset{U,V}{\text{maximize}} \quad \sum_{j=1}^k \mu_j u_j^T X v_j - \sum_j \lambda_j \|v_j\|_1 \quad \text{subject to} \quad U \in \mathcal{B}(n, k), V \in \mathcal{V}(p, k),$$

where V contains the PC loadings, and u_j and v_j are the j th column of U and V respectively, and μ_j is the weight for the j th sparse PC, and λ_j is the sparsity tuning parameter for the j th sparse PC. The algorithm of GPower fundamentally deals with sparse PCs individually, which prohibits orthogonal rotations (on V).

SPCArt [Hu et al., 2016] SPCArt is the first (to our knowledge) sparse PCA method that concerns orthogonal rotations in its formulation. It searches for sparse PCs by directly approximating the singular vectors (as opposed to minimizing the reconstruction error or maximizing the explained variance),

$$\underset{Y,R}{\text{minimize}} \quad \|V - YR\|_F^2 + \lambda\|Y\|_1 \quad \text{subject to } Y \in \mathcal{V}(p, k), R \in \mathcal{U}(k),$$

where $V \in \mathcal{V}(p, k)$ contains the top k singular vectors of X , and Y contains the sparse loadings. Conceptually, introducing an orthogonal rotation (R) allows a larger searching space for Y . However, the algorithm of SPCArt does not specifically update R to promote sparsity (e.g., minimize $\|Y\|_1$ as in SCA); instead, SPCArt simply computes R so as to align the polar of V and Y (i.e., $\hat{R} = \text{polar}(Y^T V)$). As such, the performance of SPCArt could be sensitive to the initialization of Y . Empirically, SPCArt yields results that are nearly comparable to the GPower based method, as concluded by the authors.

3.2 Sparse coding and independent component analysis

Sparse coding concerns low-rank representations of individual samples. We view it as a variant of PCA, where we presume the component scores to be sparse. Recall that the scores are the representations of individual data points in \mathbb{R}^k , where k is the number of PCs. In particular, presuming sparse scores implies that each data point is correlated with only a small subset of PCs. Sparse coding is useful to generate simple representations of individual data points, and the basis of such representations (i.e., PCs) usually provide scientific insights. For example, sparse coding of natural images recovers the common understanding of how the primary visual cortex in mammalian perceives scenes (see Section 5.1 for an example).

The SCA algorithm can be used to solve sparse coding. This is because, similar to SCA, sparse coding can be viewed as a special case of the SMA problem. To see this, simply

omit the sparsity constraint on Y in (12),

$$\begin{aligned} & \underset{Z, B, Y}{\text{minimize}} && \|X - ZBY^T\|_F \\ & \text{subject to} && Z \in \mathcal{B}(n, k), Y \in \mathcal{B}(p, k), \mathcal{P}_1(Z) \leq \gamma_z \end{aligned}$$

Here, Z contains the sparse scores, and BY^T contains the basis of sparse coding. To solve sparse coding, we apply the SCA algorithm (Algorithm 2) to the transposed data matrix, X^T . In doing this, the output of the algorithm is actually an estimate of sparse component scores for the original data matrix.

More broadly, independent component analysis (ICA) is widely applied for sparse coding in the signal processing literature. Despite the different motivations, sparse PCA on a transposed data matrix appears to perform very similarly to sparse ICA on the original data. We elaborate on this in Supplementary Section D and apply SCA to blind source separation of images.

4 Simulation studies

In this section, we compare several sparse PCA methods using simulated data. Specifically, we focused on (1) their ability of explaining variance in the data, (2) the robustness against varying sparsity parameters, and (3) the computational speed. We selected SPCA, SPC, GPower, the SPCAvRP method recently proposed by Gataric et al. [2020], SCA, and another variant of SCA which deploys the absmin rotation (SCA-absmin, see Remark 3 of Section 2.2.3). For SCA and SCA-absmin, we implemented the algorithms in R.⁵ For SPCA, SPC, and SPCAvRP, we invoked the original R packages `elasticnet`, `PMA`, and `SPCAvRP` respectively. The implementation of GPower (in `MATLAB`) was obtained from the authors' website. For all the iterative methods, we specified maximum number of iterations to 1,000

⁵We provide an R package `epca`, for **e**xploratory **p**roduct **c**omponent **a**nalysis, which implements SCA and SMA with various algorithmic options. The package is available from CRAN (<https://CRAN.R-project.org/package=epca>).

and the stopping (convergence) criterion to 10^{-5} . Overall, our numerical experiments showed that the SCA algorithm converges faster and produces more robust sparse PCs that capture a larger amount of variance in the data.

4.1 Proportion of variance explained

In this simulation, we compared the abilities of sparse PCA methods in explaining variance in the data. To this end, we simulated 30 data matrices with $n = 100$ observations and $p = 100$ variables from the following low-rank generative model:

$$X = SY^T + E,$$

where $S \in \mathbb{R}^{100 \times 16}$ contains the component scores, and $Y \in \mathbb{R}^{100 \times 16}$ contains the loadings of sparse PCs, and $E \in \mathbb{R}^{100 \times 100}$ is some noise. To generate S , we randomly sampled $U \in \mathcal{V}(100, 16)$ and $V \in \mathcal{U}(16)$ and set $S = U\Sigma V^T$, where Σ is a diagonal matrix with the diagonals $\sigma_l = 10 - \sqrt{l}$ for $l = 1, 2, \dots, 16$. To simulate a sparse Y , we took a random element from $\mathcal{V}(100, 16)$, then soft-threshold its elements with sparsity parameter $\gamma = 20$ (i.e., T_{20} as defined in Equation (9)). Note that, it is unnecessary to re-scale the columns of loadings to unit length, because the column of S can absorb these scalars. Lastly, the elements in E were drawn independently from the normal distribution, $E_{ij} \sim N(0, 0.1^2)$.

We applied the six sparse PCA methods to each simulated data matrix X with $k = 2, 4, 6, \dots, 16$. For each k , we imposed the same ℓ_1 -norm constraint on the sparse loadings for all methods. Specifically, for SCA, and SPC, we directly configured the sparsity controlling parameters to $2.5k$. As for SPCA, GPower and SPCAvRP, to ensure a fair comparison, we tuned the parameters such that the returned loadings all have the same ℓ_1 norm of $2.5k$. To evaluate sparse PCs, we define the cumulative proportion of variance explained (PVE) by the first k sparse PCs as $\|X_Y\|_F^2$, where $X_Y = XY(Y^TY)^{-1}Y^T$ [Shen and Huang, 2008]. Note that the PVE by sparse PCs is upper bounded by that of traditional PCs (no sparsity constraint). Therefore, we also applied PCA to X for comparison. Figure 3 displays the

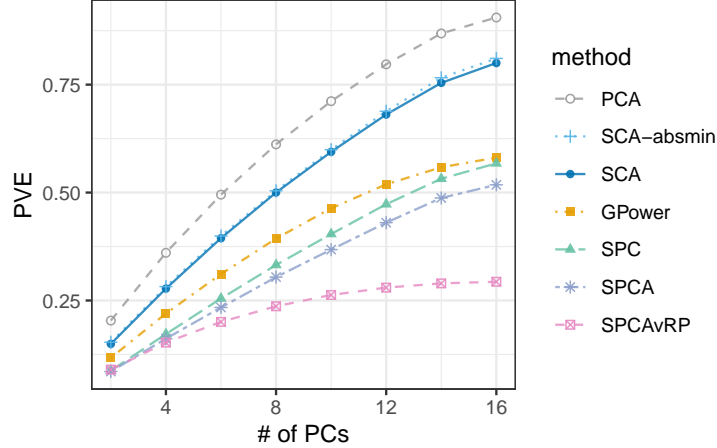


Figure 3: Comparisons of sparse PCA methods using simulated data. The proportion of variance explained (PVE) by sparse principal components (PCs) with the number of targeted PCs varying from 2 to 16.

mean PVE for different PCA methods, varying the requested number of PCs from 2 to 16. It can be seen that SPCAvRP and SPCA explained less than half of the PVE by PCA, and that GPower and SPC both exhibited some improvements over SPCA. For GPower, we tested both the single-unit and the block versions, but the block version often converged to a defective solution with some columns decaying to all zeros. This happened when the number of targeted PCs went above 5 in this simulation. Overall, SCA performed the best among sparse PCA methods and were the closest to PCA. In addition, the SCA algorithm converged with fewer iterations than the other sparse PCA methods (see Table 1 for a comparison when $k = 16$). We also observed that using the varimax rotation (SCA), the algorithm was more computationally efficient than using the absmin rotation (SCA-absmin).

4.2 Robustness against tuning parameters

This simulation study investigates the robustness of sparse PCA to the choice of sparsity parameters. For this, we applied sparse PCA to detect communities in networks (or graph partitioning) [see, e.g., Fortunato, 2010], using the graph adjacency matrix (see the

Method	# of iterations	Mean run time (s)	Environment
SCA	10 ~ 65 (all PCs)	0.96	R
SPC	25 ~ 1,000 (each PC)	1.21	R
GPower	30 ~ 150 (each PC)	0.19	MATLAB
SPCA	470 ~ 920 (all PCs)	56.30	R
SPCAvRP	/	28.67	R
SCA-absmin	/	23.5	R

Table 1: Comparison of the computational efficiency of sparse PCA methods. Each method is tasked to find 16 PCs on a single CPU (2.50GHz). SPCAvRPs is not iterative (yet is parallelizable), hence the number of iterations is not applicable. The absmin rotation is less efficient, so we halted the algorithm of SCA-ABSMIN after the 15th iteration.

definition below) as input. This application is possible thanks to the recent consistency results [Rohe and Zeng, 2020] showing that under the stochastic block model [SBM, see for example Holland et al., 1983], the support of each sparse PC estimates the membership (indicator) of one community. Hence, we could evaluate sparse PCs by examining their support.

We simulated 30 undirected graphs with $n = 900$ nodes and four equally sized blocks from the SBM. Under the SBM, the edge between node i and j is sampled from the Bernoulli distribution, $\text{Bernoulli}(B_{z(i),z(j)})$, where $z(i) \in \{1, 2, 3, 4\}$ is the membership of node i , and

$$B = 0.05 \times \begin{bmatrix} 0.6 & 0.2 & 0.1 & 0.1 \\ 0.2 & 0.7 & 0.05 & 0.05 \\ 0.1 & 0.05 & 0.6 & 0.25 \\ 0.1 & 0.05 & 0.25 & 0.6 \end{bmatrix}$$

is the block connectivity matrix. Under this setting, the expected number of edges connected to each node is 45. For each simulated graph, we defined the adjacency matrix $A \in \{0, 1\}^{n \times n}$ with $A_{ij} = 1$ if and only if i and j are connected.

We applied SCA, SPC, and GPower⁶ to each of the 30 simulated adjacency matrices with $k = 4$. We varied the sparsity parameter γ to take value in $\{18, 24, 36, 48, 60, 66\}$. For

⁶Since SPCA and SPCAvRP performs worse than SPC and GPower [Zou and Xue, 2018], we excluded the two methods in this simulation for simplicity.

SPC, we required each of the four PCs to have ℓ_1 norm $\gamma/4$. As for GPower, we tuned its parameters such that the returned loading matrix has the ℓ_1 norm of γ . Figure 4 depicts the estimated loadings returned by SCA and SPC. On the left two columns of panels ($\gamma = 48$ and 36), the supports of the four sparse PCs were well separated and indicated block memberships. This suggested that we could use the loadings to cluster nodes and quantitatively assessed the quality of sparse PCA methods. Specifically, we assigned node i to cluster j if Y_{ij} is the largest absolute value in the i th row of Y , that is, $|Y_{ij}| > |Y_{il}|$ for all $l \neq j$. In the case of ties or all-zero rows, the cluster label is randomly assigned. For each estimate, let $C \in \{1, 2, 3, 4\}^n$ contain the assigned cluster labels and $C^* \in \{1, 2, 3, 4\}^n$ contain the true labels. Define the accuracy as

$$\text{Accuracy}(C, C^*) = \max_{\pi \in \mathcal{P}(4)} \left\{ \frac{1}{n} \sum_{i=1}^n \mathbb{1}(\pi(C_i) = C_i^*) \right\},$$

where $\mathcal{P}(4)$ contains all the possible permutation functions of the set $\{1, 2, 3, 4\}$, and $\mathbb{1}(x)$ is the indicator function of x . We used the accuracy to assess the quality of the sparse PCA solutions. Figure 5 depicts the accuracy of the three methods with varying sparsity parameters. It can be seen that the performance of GPower and SCA were less affected by the changing of sparsity parameter, while SPC was profoundly influenced. As γ became smaller, SPC quickly lost its power in community detection, suggesting that SPC is more sensitive to the choices of tuning parameter. Although less sensitive to the change in γ , GPower produced poorer estimation of sparse PCs, with the accuracy slightly better than random guesses (accuracy = 0.25). Overall, SCA yielded higher accuracy with smaller deviation compared to the others, suggesting that SCA is less dependent on the choice of sparsity parameters.

In this example, SCA outperforms SPC because it finds a better optimization solution. This comparison could be made difficult by the fact that they have different objective functions. However, in this case, even though SCA is optimizing a different objective function, it outperforms SPC at *optimizing the SPC objective function*. Table 2 lists the

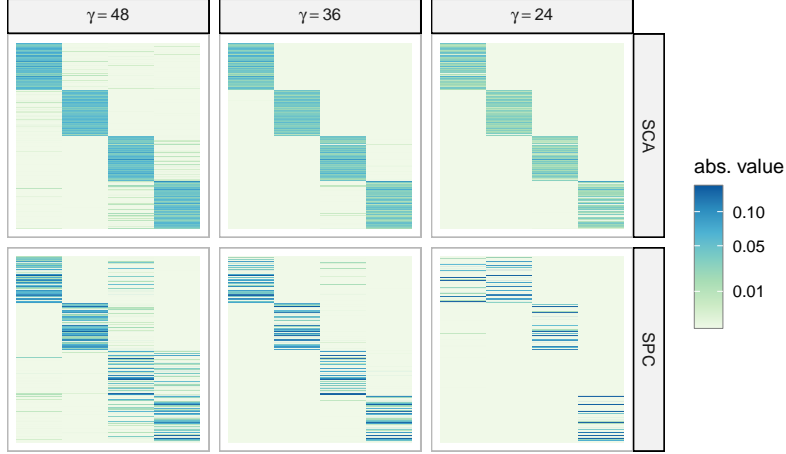


Figure 4: Comparisons of SCA and SPC using simulated network data. Heat maps of the loadings (900×4 matrices) returned by SCA and SPC using three different sparsity parameters ($\gamma = 24, 36, 48$). In each heat map, rows correspond to nodes, which are grouped by the true community membership, and each column corresponds to one sparse PC. The color shade indicates the absolute of loadings.

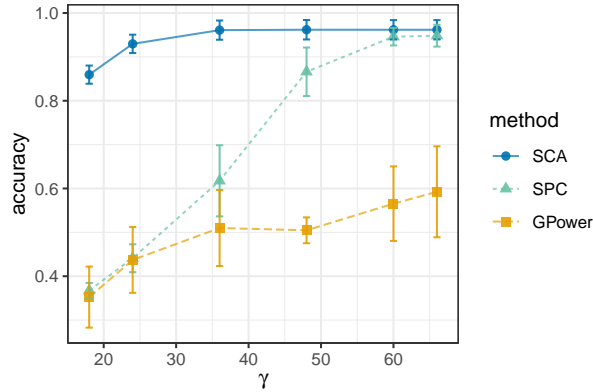


Figure 5: Comparisons of sparse PCA methods using simulated network data. The accuracy of SCA, GPower, and SPC in community detection using various sparsity parameters (γ). Each point indicates the mean accuracy across 30 replicates, and the error bar indicates the standard deviation of the evaluated accuracy.

	$\gamma = 18$	$\gamma = 24$	$\gamma = 36$	$\gamma = 48$	$\gamma = 60$	$\gamma = 66$
Using SCA solution	191.47	323.36	1135.03	1906.25	2554.86	2783.73
Using SPC solution	544.81	705.01	1029.04	1195.91	1334.67	1423.95

Table 2: Comparison of the SPC objective values, $\sum_{i=1}^4 (u_i^T A v_i)^2$ (see Equation (14)), evaluated using the output of the SCA and SPC algorithms with various sparsity parameter (γ).

objective values of SPC (Equations (14)) evaluated using the solutions of the SCA and SPC algorithms with various γ . When $\gamma \in \{36, 48, 60, 66\}$, the SCA algorithm outputs a solution that achieves a higher value of the SPC objective, suggesting that the SPC algorithm is likely to return local optima.

5 Applications

In this section, we applied SCA to real data. The first application is the sparse coding of natural images. It illustrates the utility of sparse PCA as independent component analysis. Supplementary Section D.1 contains another application of SCA to blind source separation of images. Next, we demonstrate the ability of SCA in handling high-dimensional problems (i.e., $p > n$) through a transcriptome sequencing dataset and a targeted sample of Twitter friendship network. These datasets are of large scale. To our knowledge, no other current implementations of sparse PCA can efficiently handle a large matrix at the scale. As such, we will restrict our discussion to SCA.

5.1 Sparse coding of images

Low-level visual layers, such as retina, the lateral geniculate nucleus, and the primary visual cortex (V1) are shared processing components in mammalian. The receptive fields in the V1 can be characterized as being spatially localized, oriented and bandpass (i.e., selective to structure at different spatial scales). To understand V1, one line of research focuses on finding sparse and linearly independent codes for natural images, which provides an efficient representation for later stages of processing [Field, 1994, Olshausen and Field, 1996, Bell and Sejnowski, 1997]. This type of research is based on the hypothesis of sparse coding, that is, any perceived scenes can be synthesized via the linear combination of some small subsets of basis images [Lee et al., 2006, Gregor and LeCun, 2010]). In this application, we show that sparse PCA produces a set of bases for natural images that resembles those found in Olshausen and Field [1996].

We utilized ten natural images from [Olshausen and Field \[1996\]](#), each of which contains 512×512 pixels. We followed the same whitening process as described by the authors. Next, we randomly sampled a total of 12,000 small image patches the ten images, where each patch contains 16×16 pixels. This was followed by a centering step that subtracts each pixel by the mean of all 256 pixels. We vectorized each patch of image and put them into the rows of a data matrix, $X \in \mathbb{R}^{n \times p}$, where $n = 12,000$ and $p = 256$. Finally, we applied SCA to the transposed data matrix, X^T , to find 49 sparse PCs ($k = 49$) with the default sparsity parameter, $\gamma = \sqrt{pk}$ (Note that this is sparse coding). In particular, for the varimax rotation, we normalized the rows to unit length rescaled them afterward, as recommended by [Kaiser \[1958\]](#). In the output of SCA, the estimated scores $S \in \mathbb{R}^{p \times k}$ contains the basis images, and the estimated sparse loadings $Y \in \mathbb{R}^{n \times k}$ encodes how the basis images are linearly combined to form each image patch (i.e., Y contains the linear coefficients).

Figure 6 displays the 49 image bases returned by PCA and SCA, where each image represents one column of S (transformed into a 16×16 array). For SCA, all of the basis images appeared to exhibit simple patterns, such as lines and edges. As for PCA, the oriented structure in the first few basis images does not arise as a result of the oriented structures in natural images, yet more likely because of the existence of those components with low spatial frequency [[Field, 1987](#)].

5.2 Analysis of single-cell gene expression data

Single-cell transcriptome sequencing (scRNA-seq) provides high-throughput transcriptome expression quantification at individual cell level. It has been widely used across biological disciplines. For example, patterns of gene expression can be identified through clustering analysis. This helps uncover the existence of rare cell types within a cell population that have never been seen [[Plasschaert et al., 2018](#), [Montoro et al., 2018](#)]. In this application, we aimed to use SCA to extract the sparse PCs of genes that characterize some known cell types.

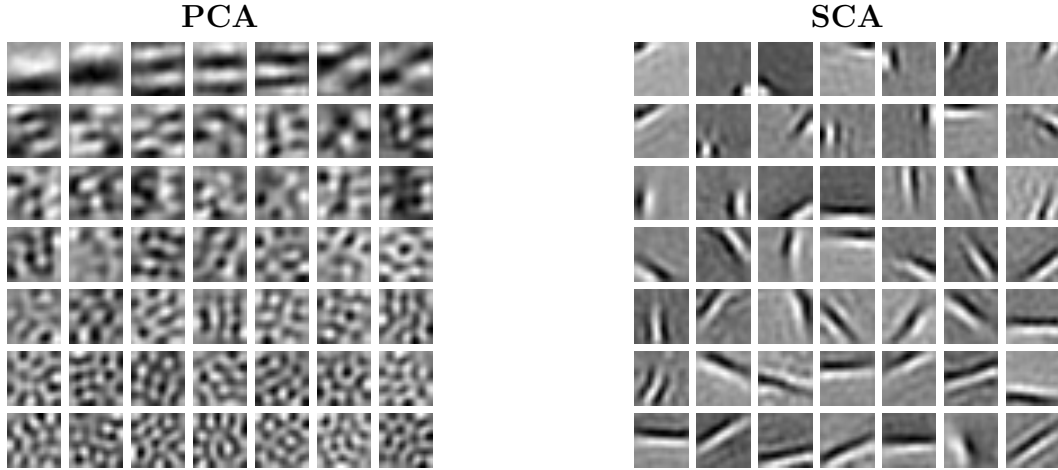


Figure 6: Sparse image encoding using PCA (left) and SCA (right). For both method, shown are the 49 image bases (i.e., component scores) extracted from natural images. Each image basis is in 16×16 pixel.

For this application, we used the human pancreatic islet cell data from [Baron et al. \[2016\]](#). We removed the genes that do not exhibit variation across all cells (i.e., zero standard deviation) and removed the cell types that contain fewer than 100 cells. This resulted in a data matrix $X \in \mathbb{R}^{n \times p}$ of $n = 8,451$ cells across nine cell types and $p = 17,499$ genes, with X_{ij} measuring the expression level of gene j in cell i . X is sparse; it contains 10.8% non-zero elements. We applied SCA on X to find $k = 9$ sparse gene PCs. We set the sparsity parameter to $\gamma = \log(pk) \approx 12$, as we aimed for particularly sparse PCs (i.e., each PC is consist of a small number of genes). The algorithm took about 5 minutes (24 iterations) to complete on a single processor (3.3GHz). As a result, each column of the loading matrix contains a small number of non-zero elements, suggesting that most of the gene PCs consist of one or a few genes. Table 3 lists the names of these genes for each PCs. For example, the PC 2 consists of only one gene, SST. Despite the simple structure of PCs, these PCs picked up informative gene markers for individual cell types. To see this, we calculated the scores for each cell using the 9 PCs (That is, each cell gets 9 scores, each of which corresponds to one of the nine PCs). Figure 7 displays the box plots of the scores stratified by cell type. For example, the expression of the SST gene (which solely composes

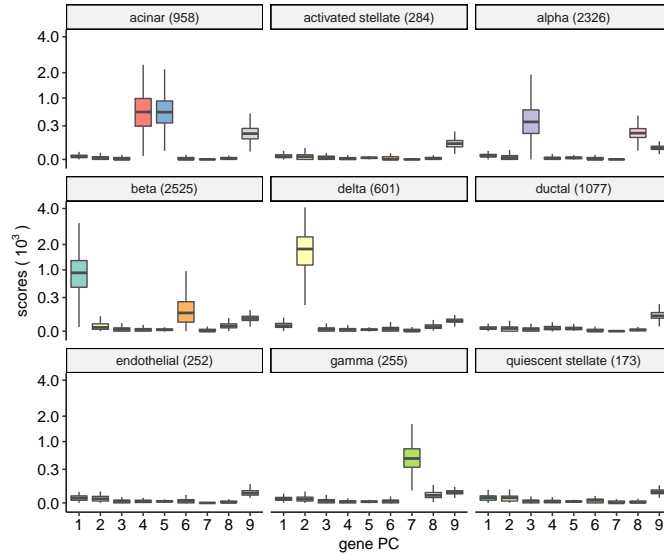


Figure 7: Scores of sparse gene principal components (PCs) stratified by cell types. Each panel displays one of nine cell types with the names of cell types and the number of cells reported on the top strips. For each cell type, a box depicts the component scores for nine sparse gene PCs.

the 2nd PC) identifies the “delta” cells. This result highlights the power of scRNA-seq in capturing cell-type specific information and suggests the applicability of our methods to high-dimensional biological data.

5.3 Clustering of Twitter friendship network

This application serves in a grand efforts of ours to study political communication on social media, like Twitter. The information on Twitter is organized so that users primarily read the tweets of their “friends.” In order to select content, a user can freely “follow” (and “unfollow”) any other accounts, and we call these other accounts the friends of it. Thanks to this design, the communication on Twitter can be contextualized by the friendship network. As such, we hypothesize that user’s community membership in the network offers the context of user’s opinion expression on social media [Zhang et al., 2021]. To study the hypothesis, a key step is to cluster Twitter accounts using their friendship network. In this section, we demonstrate large-scale network clustering using sparse PCA.

PC	# of genes	Gene name(s)
1	1	INS
2	1	SST
3	1	GCG
4	8	CTRB2, REG1A, REG1B, REG3A, SPINK1 ...
5	15	CELA3A, CPA1, CTRB1, PRSS1, PRSS2 ...
6	1	IAPP
7	1	PPY
8	3	CLU, GNAS, TTR
9	61	ACTG1, EEF1A1, FTH1, FTL, TMSB4X ...

Table 3: Sparse gene PCs estimated by SCA. For each gene PC, the number of genes (i.e., the number of non-zeros in the loadings) and the top 5 genes according to the absolute loadings are reported.

For this application, we collected a targeted sample from the Twitter friendship network in August 2018 [Chen et al., 2020]. In this sample, there are $n = 193,120$ Twitter accounts who follow a total of $p = 1,310,051$ accounts, after filtering out the accounts with few followers or followings. We defined the graph adjacency matrix $A \in \{0, 1\}^{n \times p}$ with $A_{ij} = 1$ if and only if account i follows account j .⁷ This resulted in a sparse A with about 0.02% entries being 1. We applied SMA to A with $k = 100$ and default sparsity parameters. This analysis was computationally tractable; one iteration of the SMA algorithm took about 54 minutes on a single processor (2.5GHz), thanks to the efficient algorithm that computes the sparse SVD [Baglama and Reichel, 2005]. Figure 2 displays seven example columns of Y . Using the output $Z \in \mathbb{R}^{n \times k}$ and $Y \in \mathbb{R}^{p \times k}$ from SMA, the clusters of Twitter accounts were determined as follows (same as in Section 4.2): the i th row account of A was assigned to the l th row cluster if Z_{il} was the greatest in the i th row of Z , that is, $|Z_{il}| \geq |Z_{il'}|$ for all $l' = 1, 2, \dots, k$, and the j th column account of A was assigned to the l th column cluster if Y_{jl} was the greatest in the j th row of Y , $|Y_{jl}| \geq |Y_{jl'}|$ for all $l' = 1, 2, \dots, k$. Upon detailed evaluation of these clusters, we showed that our clustering of Twitter accounts formed

⁷The columns of A are not centered nor scaled. One alternative is to use the normalized version of A . For example, define the regularized graph Laplacian as $L \in \mathbb{R}^{n \times p}$ with $L_{ij} = A_{ij} / \sqrt{(r_i + \bar{r})(c_j + \bar{c})}$, where $r_i = \sum_j A_{ij}$ is the sum of the i th row of A , $c_j = \sum_i A_{ij}$ is the sum the j th column of A . Here, \bar{r} and \bar{c} are the means of r_i 's and c_j 's respectively. [Zhang and Rohe, 2018].

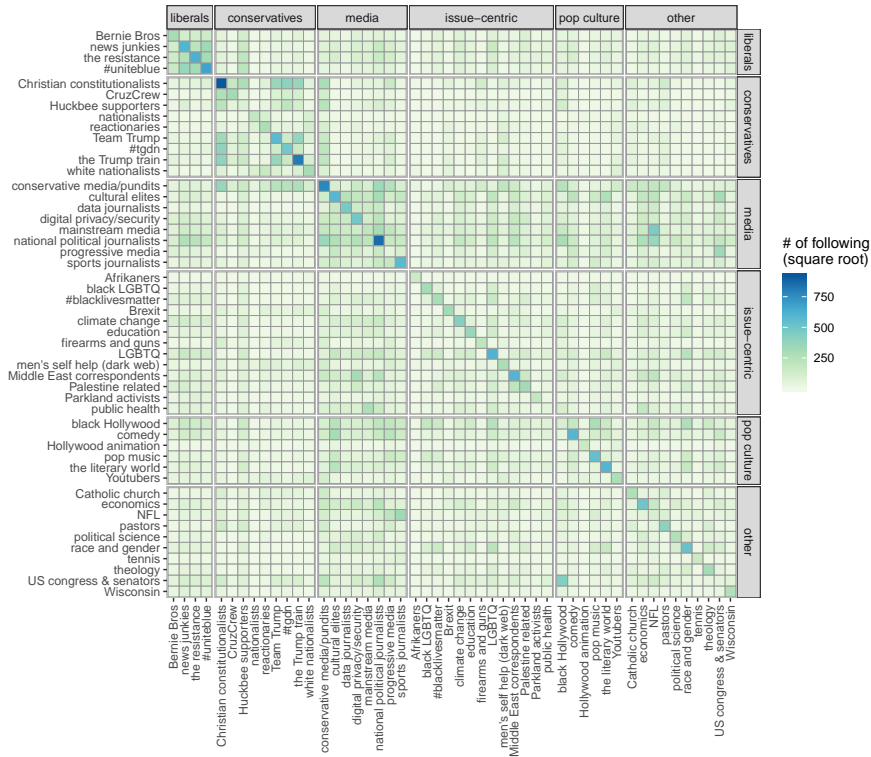


Figure 8: Heat map of friend counts between row and column clusters of Twitter accounts. Each row and column corresponds to a cluster. The row and column panels indicate cluster category, with the category names shown in the top and right strips. The color shades indicate the number of followings from the row cluster to the column cluster, after the square root transformation.

homogeneous, connected, and stable social groups [Zhang et al., 2021]. For example, we found that a user is more likely to retweet the content that originated from another member in the same clusters (p-value $< 10^{-16}$ in a χ^2 test). More interestingly, the estimated row clusters and column clusters are matched [Rohe et al., 2016], that is, the k th row cluster tends to follow the accounts in the k th column cluster. To illustrate this, we quantified the number of followings from the row clusters to the corresponding column clusters. Figure 8 displays the results for 50 selected clusters that are related to U.S. politics. It can be seen that the number of followings between each paired row and column clusters (i.e., the diagonals in Figure 8) showed marked enrichment. These results suggest the efficacy of our methods for analysis of social network data.

6 Discussions

In this paper, we introduced SCA, a new method for sparse PCA, and SMA, an extension for two-way matrix analysis. SCA differs from the existing sparse PCA methods in that it estimates column sparse PCs, that is PCs that are sparse in an orthogonally rotated basis. This is particularly useful when the singular vectors of a data matrix (or the eigenvectors of the covariance matrix) are not readily sparse. We demonstrated that it explains more variance in the data than the state-of-the-art methods of sparse PCA. In addition, the algorithm is also stable and robust against a wide choices of tuning parameters. In practice, SCA is advantageous when multiple PCs are desired because it does not require the deflation.

Acknowledgments

We thank Sündüz Keleş, Sébastien Roch, Po-Ling Loh, Michael A Newton, Yini Zhang, Muzhe Zeng, Alex Hayes, E Auden Krauska, Jocelyn Ostrowski, Daniel Conn, and Shan Lu for all the helpful discussions.

Appendices

A Technical proofs

Proof. of Proposition 1 We show that for any fixed Z and Y , the inequality holds for the minimization over B on the left-hand-side and the diagonal D on the right-hand-side,

$$\min_B \|X - ZBY^T\|_F^2 \leq \min_D \|X - ZDY^T\|_F^2.$$

In fact, the maximizer of the left-hand-side is $B^* = (Z^T Z)^{-1} Z^T X Y (Y^T Y)^{-1}$ if Z and Y are full-rank, or $B^* = (Z^T Z)^+ Z^T X Y (Y^T Y)^+$ if either Z or Y is singular, where A^+ is

the Moore–Penrose inverse of matrix A . Since B^* is not diagonal in general, the inequality follows. \square

Proof. of Lemma 1 We rewrite the objective function:

$$\begin{aligned}\|X - ZBY^T\|_F^2 &= \text{tr} \left[(X - ZBY^T)^T (X - ZBY^T) \right] \\ &= \|X\|_F^2 - 2 \text{tr} (X^T ZBY^T) + \text{tr} (B^T B) \\ &= \|X\|_F^2 - \text{tr} [B^T (2Z^T XY - B)].\end{aligned}$$

For fixed Z and Y , take the derivative of B and set it to zero. We have the optimizer $B^* = Z^T XY$ and the squared optimal value is $\|X\|_F^2 - \|Z^T XY\|_F^2$. Recognizing that $\|X\|_F^2$ is determined, the desired formulation (13) follows. \square

Remark 4 (Minimal matrix reconstruction error of PMD). *If B is constrained to a diagonal matrix in (12), then the squared minimal value is $\|X\|_F^2 - \sum_{i=1}^k d_i^2$, where $d_i = [Z^T XY]_{ii}$ for $i = 1, 2, \dots, k$.*

Proof. From the proof of Lemma 1, we have

$$\|X - ZDY^T\|_F^2 = \|X\|_F^2 - \text{tr} [D^T (2Z^T XY - D)].$$

Then, take the derivative of D and set it to zero. This yields the solution $\hat{D} = \text{diag}(d_i)$, where $d_i = [U^T XV]_{ii}$. Finally, plugging-in the maximizer \hat{D} gives the claimed optimal value. Note that $\sum_{i=1}^k d_i^2 \leq \|U^T XV\|_F^2$. \square

Proof. of Lemma 2 Suppose the low-rank SVD of $C \in \mathbb{R}^{p \times k}$ is UDV^T , where $U \in \mathcal{V}(p, k)$, $V \in \mathcal{U}(k)$, and $D \in \mathbb{R}^{k \times k}$ is diagonal. Then,

$$\|C^T X\|_F^2 = \text{tr} (X^T C C^T X) = \text{tr} (X^T U D^2 U^T X).$$

The trace quadratic form is maximized at $X^* = UR$, for any orthogonal matrix $R \in \mathcal{U}(k)$. In particular, when $R = V$, $X^* = \text{polar}(C)$. \square

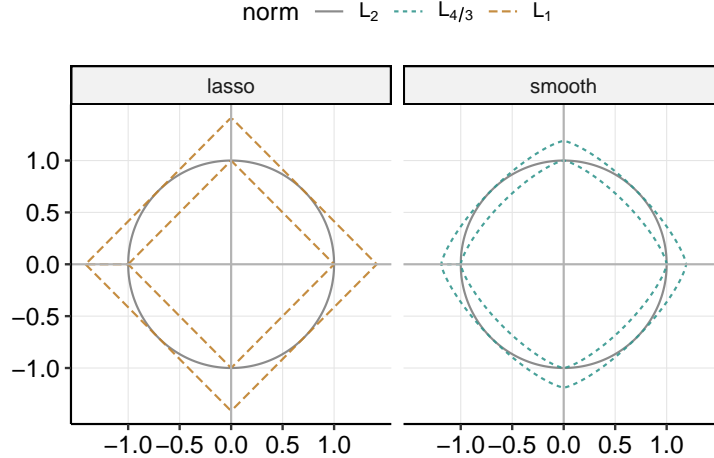


Figure 9: Comparison of the ℓ_p norms. Left (lasso): Two ℓ_1 -norm contours (brown) of 1 and $\sqrt{2}$ and the ℓ_2 -norm contour (grey) of 1. Right (smooth): $\ell_{4/3}$ -norm contours (green) of 1 and $2^{1/4}$ and the ℓ_2 -norm contour (grey) of 1.

B Choosing the sparsity parameter

The sparsity controlling parameters in SCA and SMA— γ , γ_y , and γ_z —are meaningful if they take values from a certain range, depending on the choice of ℓ_p -norm constraint. In this section, we discuss the sparsity constraint on Y ; the constraint on Z is similar. First, consider the ℓ_1 -norm constraint $\|Y\|_1 \leq \gamma$. The sparsity parameter should satisfy $k \leq \gamma \leq k\sqrt{p}$. This is for the set $\{Y \in \mathbb{R}^{p \times k} \mid \|Y\|_1 = \gamma\}$ to intersect with $\mathcal{V}(p, k)$. On the right hand side, if $\gamma > k\sqrt{p}$, any element in $\mathcal{V}(p, k)$ satisfies $\|Y\|_1 < \gamma$, so the sparsity constraint is ineffective (Figure 9: left panel). On the left hand side, if $\gamma < k$, none of the elements in $\mathcal{V}(p, k)$ satisfies $\|Y\|_1 \leq \gamma$, so the solution to (4) does not fall on $\mathcal{V}(p, k)$. Similarly, for the $\ell_{4/3}$ -norm sparsity constraint $\|Y\|_{4/3} \leq \gamma$, the sparsity controlling parameter should take value within $k^{3/4} \leq \gamma \leq p^{1/4}k^{3/4}$ (Figure 9: right panel).

In Algorithm 2, the sparsity parameter is optional. If absent, the algorithm uses a default value of $\gamma = \sqrt{pk}$ (or $\gamma_z = \sqrt{nk}$ and $\gamma_y = \sqrt{pk}$ in SMA). This is supported by our simulation results showing that the SCA algorithm is robust against various choices of γ (Section 4.2 of the paper). In addition, we observed that the default settings generally

yielded meaningful estimates in real data applications.

The sparsity parameter can also be tuned based on the data. We provide a schema for cross-validate the parameters of SCA and SMA (e.g., the approximation rank k and the sparsity parameter γ). To assess a candidate parameter, we adapt a K -fold cross-validation framework (K often takes the value 10) as previously introduced by [Wold \[1978\]](#):

- (a) Given the input data $X \in \mathbb{R}^{n \times p}$, we first construct K leave-out data matrices $X^{(1)}, X^{(2)}, \dots, X^{(K)} \in \mathbb{R}^{n \times p}$, each of which has one- K th disjoint portion of elements being randomly sampled and removed (i.e., set to zero). Let $C^{(k)}$ collect the indices of those left-out elements in $X^{(k)}$, for $k = 1, 2, \dots, K$.
- (b) Next, we apply SCA (or the SMA) to every new matrix $X^{(k)}$ with the candidate tuning parameters and obtain its low-rank approximation $\hat{X}^{(k)}$. That is, for SCA, $\hat{X}^{(k)} = X^{(K)}\hat{Y}^{(k)}[\hat{Y}^{(k)}]^\text{T}$, and for SMA, $\hat{X}^{(k)} = \hat{Z}^{(k)}\hat{B}^{(k)}[\hat{Y}^{(k)}]^\text{T}$
- (c) Finally, calculate the mean square error (MSE) of $\hat{X}^{(k)}$ over those left-out elements $C^{(k)}$, defined as

$$\text{MSE}(k) = \sum_{(i,j) \in C^{(k)}} \left(\hat{X}_{ij}^{(k)} - X_{ij} \right)^2, k = 1, 2, \dots, K.$$

We then evaluate the “goodness” of a candidate parameter by the average MSE across K leave-out data matrices.

Upon the construction of leave-out data matrices, the left-out elements are randomly sampled; this typically removes scattered entries of X , rather than trunks of adjacent ones. For example, if X is the adjacency matrix of a graph, then this procedure is akin to the edge cross-validation studied by [Li et al. \[2020\]](#). Setting the left-out elements to zero eliminates all terms in $\|Z^\text{T}XY\|_\text{F}$ that related to them. Our low-rank estimation for the missing entries is closely related to the SVD-based methods in data imputation literature [[Troyanskaya et al., 2001](#)].

C Properties of soft-thresholding

In the PRS update, the last step uses a shrinkage operator to project the rotated matrices onto the feasible set. Shrinkage operators are widely used for creating sparse structure, as it is easy to implement. The threshold value t can be found in $\mathcal{O}(\log_2(1/\varepsilon))$ time through a binary search, where ε is the convergence tolerance.

For the ℓ_1 -norm constraint (or penalty), we show that a soft-thresholding shrinkage is “appropriate.” Let $Y \in \mathcal{V}(p, k)$ and $\hat{Y} \in \mathcal{B}(p, k)$ be the two matrices before and after a shrinkage operation respectively. A direct calculation shows that given a constraint $\|\hat{Y}\|_1 \leq \gamma$, the soft-thresholding shrinkage, $\hat{Y} = T_\gamma(Y)$, minimizes $\|\hat{Y} - Y\|_F$. After the shrinkage, the objective value in (4) (i.e., explained variance) decreases by at most $\|Z^T X\|_F \|\hat{Y} - Y\|_F$. Note that we update Y fixing Z (and X).

We provide theoretical properties for the soft-thresholding, regarding preservation of orthogonality and the explained variance. Let $Y \in \mathcal{V}(p, k)$ and let $\hat{Y} = T_\gamma(Y)$ be the result of soft-thresholding Y as defined in (9).

First, we denote the included angles between any two columns of \hat{Y} and Y as θ_{ij} , for $i, j = 1, 2, \dots, k$. When it is clear, we also write θ_{ii} as θ_i for simplicity. We define the *deviation* between \hat{Y} and Y as $\sum_{i=1}^k \sin^2(\theta_i)$. The following proposition bounds the sum of deviations.

Proposition 2 (Deviation due to soft-thresholding). *If t is sufficiently small, then*

$$\sum_{j=1}^k \sin^2(\theta_j) \leq \left\| \hat{Y} - Y \right\|_F^2.$$

Proof. Let \hat{y}_i and y_i be the i th column of \hat{Y} and Y respectively. For the included angle θ_i ,

$$\begin{aligned} \cos(\theta_i) &= \hat{y}_i^T y_i / \|\hat{y}_i\|_2 \\ &= \|\hat{y}_i\|_2 + \hat{y}_i^T (y_i - \hat{y}_i) / \|\hat{y}_i\|_2 \\ &> \|\hat{y}_i\|_2. \end{aligned}$$

The last inequality results from the definition of soft-thresholding. Then, by the Pythagorean trigonometric identity, we have

$$\begin{aligned}\sin^2(\theta_i) &= 1 - \cos^2(\theta_i) \\ &< 1 - \|\hat{y}_i\|_2^2 \\ &\leq \|\hat{y}_i - y_i\|_2^2.\end{aligned}$$

The last inequality is due to the triangular inequality. Finally, summing over the columns yields the desired result. \square

Proposition 2 controls the deviation with the Frobenius norm of $Y - \hat{Y}$. Since the columns of Y are mutually orthogonal, for any two columns of \hat{Y} , we have

$$|\hat{y}_i^T \hat{y}_j| \leq \sin(\theta_j + \theta_i) \|\hat{y}_i\|_2 \|\hat{y}_j\|_2$$

assuming $\theta_i + \theta_j \leq \pi/2$. Hence, a small deviation indicates that the orthogonality of \hat{Y} is conserved after soft-thresholding.

Next, we investigate the change in explained variation due to soft-thresholding. Define the explained variance (EV) of a data matrix X by the loading matrix Y as $\text{EV}(Y) = \|XY\|_F$. The following proposition bounds the EV for \hat{Y} and is due to the Theorem 13 in [Hu et al. \[2016\]](#).

Proposition 3 (Explained variance after soft-thresholding). *If for all $1 \leq i \leq k$, $\theta_i = \theta$ and $\sum_{j=1}^k \cos(\theta_{ij}) \leq 1$, then*

$$\left(\cos^2 \theta - \sqrt{k-1} \sin 2\theta\right) \text{EV}(Y) \leq \text{EV}(\hat{Y})$$

for any data matrix X .

Proposition 3 implies that if the deviation between Y and \hat{Y} is small, then the EV of

\hat{Y} is close to that of Y ,

$$(\cos^2 \theta - \mathcal{O}(\theta)) \text{EV}(Y) \leq \text{EV}(\hat{Y}).$$

D Independent component analysis

In this section, we demonstrate the connection between sparse PCA (specifically, our SCA formulation) and independent component analysis (ICA).

ICA is motivated by blind-source (or blind-signal) separation in signal processing [see, e.g., [Georgiev et al., 2005](#), [Comon and Jutten, 2010](#)], where we observe a series of multivariate signals $X_i \in \mathbb{R}^p$ for $i = 1, 2, \dots, n$, where n is the number of observations. In ICA, there exist k independent, non-Gaussian and unobserved *source* signals underlying each observation, $Z_i \in \mathbb{R}^k$ for $i = 1, 2, \dots, n$, and each observation is a linear mixture of these source signals, this is, $X = ZM^T$ (or $X_i = Z_i M$ for $i = 1, 2, \dots, n$), where $M \in \mathbb{R}^{p \times k}$ is the *mixing* matrix. ICA aims to “un-mix” the observed X and extract Z from it. In particular, since the k source signals are independent, it is often assumed that Z ’s columns have unit length and are orthogonal to each other (i.e., $Z \in \mathcal{V}(n, k)$). The ICA literature is rich in theoretical results [[Hyvärinen and Oja, 2000](#), [Chen and Bickel, 2006](#), [Samworth and Yuan, 2012](#), [Miettinen et al., 2015](#)], and most methods for ICA (e.g. fastICA) identifies both platykurtic- and leptokurtic-sourced signals.

We consider a sparse version of ICA, sparse ICA, where Z is sparse (or the columns of Z follow leptokurtic distributions). We show that sparse ICA and sparse PCA are unified by the SMA. To see this, recall from [Section 2.3](#) that the SMA of a data matrix is ZBY^T , where Z and Y are both sparse but B . We interpret the SMA for the two modern multivariate data analysis:

Sparse PCA For sparse PCA, we treat Y as the sparse loadings, and ZB together as the component scores.

Sparse ICA For sparse ICA, the sparse source signals (or the independent components) are the columns of Z , the mixing matrix is BY^T .



Figure 10: Blind image signal separation using SCA. The three panel rows display three source images, three linear mixtures of the source images, and the three separated images using SCA.

It can be seen that both sparse PCA and sparse ICA seek a sparse component in the data: sparse PCA extracts them for the column space (Y), while ICA the row space (Z). Hence, performing sparse PCA to the transposed input data matrix actually accomplishes sparse ICA to the original data. This highlights the similarities between sparse PCA and sparse ICA.

D.1 Example: Blind source separation with SCA

We apply SCA to the blind source separation of image data [Comon and Jutten, 2010]. For example, suppose the source signals are individual images, and a sensor senses several mixed images, each an linear mixture of the sources. The objective is then to identify the source images from the observed ones (i.e., to decipher the linear coefficients).

We selected three 512×512 -pixels pictures of diverse genres from the internet (Figure

10, the first row). The sample excess kurtosis of the images are 1.53, 3.32, and -0.45 respectively. Next, we generated three ($n = 3$) mixtures of the original images, with the linear coefficients randomly drawn from the uniform distribution, $\text{Unif}(0,1)$. The three mixed images are displayed in the second row of Figure 10. For sparse PCA, we vectorize the mixed images (that is 512^2 -pixels) and put them in a shallow matrix $X \in \mathbb{R}^{n \times p}$, where $p = 262,144$. This matrix is then input to SCA (Algorithm 2) for three sparse PCs ($k = 3$), with the sparsity parameter γ set to \sqrt{nk} . The resulting sparse loadings $Y \in \mathbb{R}^{p \times k}$ contains the three separated source images and the scores $S \in \mathbb{R}^{n \times k}$ decodes the mixing coefficients. The third row in Figure 10 displays the three separated images (i.e., the three rows of Y .) The clean-cut identification of the source images suggests that sparse PCA is capable of extracting sparse and independent components from the data.

D.2 Algorithmic comparisons

Another insight for sparse PCA and sparse ICA can be gleaned from their algorithms. In this section, we demonstrate that the fastICA algorithm [Hyvarinen, 1999] and our SCA algorithm are both closely related to kurtosis [Mardia, 1970].

The fastICA algorithm finds Z in two steps. The first step is to pre-process X . The pre-processing of centering and whitening (see, e.g., Comon [1994]) results in the leading k left singular vectors $\hat{U} \in \mathcal{V}(n, k)$. The second steps searches for an orthogonal rotation that maximize the non-gaussianity of $\hat{U}R$, as measured by the approximation of negentropy,

$$\underset{R}{\text{maximize}} \quad \sum_{j=1}^k \left\{ G([\hat{U}R]_{.j}) - G(\nu) \right\}^2 \quad \text{subject to } R \in \mathcal{U}(k), \quad (15)$$

where $G(x)$ is a non-quadratic function for $x \in \mathbb{R}^n$, and $\nu \sim \text{N}(0, I_n)$ is the multivariate standard Gaussian vector. Finally, $\hat{U}\hat{R}$ is the fastICA estimate for Z , where \hat{R} is the solution to (15). Hyvarinen [1999] noted that setting $G(x) = \|x\|_4^4/n$, the optimization in

(15) takes the form⁸

$$\underset{R}{\text{maximize}} \quad \sum_{j=1}^k \text{kurt}^2([UR]_{\cdot j}) \quad \text{subject to } R \in \mathcal{U}(k), \quad (16)$$

where $\text{kurt}(x)$ is the sample excess kurtosis of $x \in \mathbb{R}^n$ and is defined as $\text{kurt}(x) = n \sum_{i=1}^n (x_i - \bar{x})^4 / (\sum_{i=1}^n (x_i - \bar{x})^2)^2 - 3$, where $\bar{x} = \sum_{i=1}^n x_i / n$ is the mean. It can be seen from (16) that fastICA produces either leptokurtic ($\text{kurt}(x) > 0$) or platykurtic ($\text{kurt}(x) < 0$) estimation for the columns of Z , because of the squared kurtosis in the objective function. This primarily explains that fastICA allows both platykurtic- and leptokurtic-sourced signals.

As for SCA, the algorithm uses the varimax rotation to find the orthogonal rotation. Suppose $Y \in \mathcal{V}(n, k)$. Since the sum of squares of Y 's columns are constant, $\sum_{j=1}^k Y_{ij}^2 = 1$, maximizing the varimax rotation is equivalent to maximizing the sum of sample kurtosis of Y 's columns,

$$C_{\text{varimax}}(Y) = \sum_{j=1}^k \text{kurt}(Y_{\cdot j}) + \text{constant}.$$

This suggests that the varimax rotation in SCA promotes some leptokurtic columns in the loading Y of sparse PCs. Note that any sparse distribution is leptokurtic (see Theorem 2.1 of [Rohe and Zeng \[2020\]](#)). Hence, SCA generates specifically sparse PCs.

In many applications of ICA, the number of independent components and the number of observed variables are the same (i.e., $p = k$), in which case, the mixing matrix is square. The $p = k$ regime is generally challenging. As such, many theoretical results presume no or very little noise in X , in order for estimating guarantees. By contrast, sparse PCA typically presumes the data to comprise noise and the statistical model usually contain a noise term. In addition, it is showed that sparse PCA is consistent even when the observed data is high-dimensional (i.e., p grows at the same rate as n) or sparse by itself (i.e. contains many zeros) [[Rohe and Zeng, 2020](#)], while it is unclear yet whether ICA is consistent or not under these settings.

⁸The authors also suggested different forms of $G(x)$.

References

- Arash A Amini and Martin J Wainwright. High-dimensional analysis of semidefinite relaxations for sparse principal components. *The Annals of Statistics*, 37(5B):2877–2921, 2009.
- James Baglama and Lothar Reichel. Augmented implicitly restarted lanczos bidiagonalization methods. *SIAM Journal on Scientific Computing*, 27(1):19–42, 2005.
- Maayan Baron, Adrian Veres, Samuel L Wolock, Aubrey L Faust, Renaud Gaujoux, Amedeo Vetere, Jennifer Hyoje Ryu, Bridget K Wagner, Shai S Shen-Orr, Allon M Klein, et al. A single-cell transcriptomic map of the human and mouse pancreas reveals inter- and intra-cell population structure. *Cell Systems*, 3(4):346–360, 2016.
- Anthony J Bell and Terrence J Sejnowski. The “independent components” of natural scenes are edge filters. *Vision Research*, 37(23):3327–3338, 1997.
- Coen A Bernaards and Robert I Jennrich. Gradient projection algorithms and software for arbitrary rotation criteria in factor analysis. *Educational and Psychological Measurement*, 65(5):676–696, 2005.
- Quentin Berthet and Philippe Rigollet. Optimal detection of sparse principal components in high dimension. *The Annals of Statistics*, 41(4):1780–1815, 2013.
- T Tony Cai, Zongming Ma, and Yihong Wu. Sparse PCA: Optimal rates and adaptive estimation. *The Annals of Statistics*, 41(6):3074–3110, 2013.
- John B Carroll. An analytical solution for approximating simple structure in factor analysis. *Psychometrika*, 18(1):23–38, 1953.
- Aiyu Chen and Peter J Bickel. Efficient independent component analysis. *The Annals of Statistics*, 34(6):2825–2855, 2006.
- Fan Chen, Yini Zhang, and Karl Rohe. Targeted sampling from massive block model graphs with personalized PageRank. *Journal of the Royal Statistical Society: Series B (Statistical Methodology)*, 82(1):99–126, 2020.
- Pierre Comon. Independent component analysis, a new concept? *Signal Processing*, 36(3):287–314, 1994.
- Pierre Comon and Christian Jutten. *Handbook of Blind Source Separation: Independent component analysis and applications*. Academic Press, Oxford, UK, 2010.
- Alexandre d’Aspremont, Laurent El Ghaoui, Michael I Jordan, and Gert R G Lanckriet. A direct formulation for sparse PCA using semidefinite programming. *SIAM Review*, 49(3):434–448, 2007.

- David L Donoho. De-noising by soft-thresholding. *IEEE Transactions on Information Theory*, 41(3):613–627, 1995.
- David J Field. Relations between the statistics of natural images and the response properties of cortical cells. *Journal of the Optical Society of America A*, 4(12):2379–2394, 1987.
- David J Field. What is the goal of sensory coding? *Neural Computation*, 6(4):559–601, 1994.
- Santo Fortunato. Community detection in graphs. *Physics Reports*, 486(3-5):75–174, 2010.
- Kyle A Gallivan and PA Absil. Note on the convex hull of the Stiefel manifold. *Florida State University*, 2010.
- Milana Gataric, Tengyao Wang, and Richard J. Samworth. Sparse principal component analysis via axis-aligned random projections. *Journal of the Royal Statistical Society: Series B (Statistical Methodology)*, 82(2):329–359, 2020. doi: 10.1111/rssb.12360.
- Pando Georgiev, Fabian Theis, and Andrzej Cichocki. Sparse component analysis and blind source separation of underdetermined mixtures. *IEEE Transactions on Neural Networks*, 16(4):992–996, 2005.
- Karol Gregor and Yann LeCun. Learning fast approximations of sparse coding. In *Proceedings of the 27th International Conference on International Conference on Machine Learning*, ICML’10, page 399–406, Madison, WI, USA, 2010. Omnipress.
- Paul W Holland, Kathryn Blackmond Laskey, and Samuel Leinhardt. Stochastic block-models: First steps. *Social Networks*, 5(2):109–137, 1983.
- Roger A Horn and Charles R Johnson. *Matrix Analysis*. Cambridge University Press, Cambridge, UK, 1985.
- Harold Hotelling. Analysis of a complex of statistical variables into principal components. *Journal of Educational Psychology*, 24(6):417, 1933.
- Zhenfang Hu, Gang Pan, Yueming Wang, and Zhaohui Wu. Sparse principal component analysis via rotation and truncation. *IEEE Transactions on Neural Networks and Learning Systems*, 27(4):875–890, 2016.
- Aapo Hyvarinen. Fast and robust fixed-point algorithms for independent component analysis. *IEEE Transactions on Neural Networks*, 10(3):626–634, 1999.
- Aapo Hyvärinen and Erkki Oja. Independent component analysis: algorithms and applications. *Neural Networks*, 13(4-5):411–430, 2000.

- JNR Jeffers. Two case studies in the application of principal component analysis. *Journal of the Royal Statistical Society: Series C (Applied Statistics)*, 16(3):225–236, 1967.
- Robert I Jennrich. A simple general procedure for orthogonal rotation. *Psychometrika*, 66(2):289–306, 2001.
- Iain M Johnstone and Arthur Yu Lu. On consistency and sparsity for principal components analysis in high dimensions. *Journal of the American Statistical Association*, 104(486):682–693, 2009.
- Ian T Jolliffe. Rotation of principal components: choice of normalization constraints. *Journal of Applied Statistics*, 22(1):29–35, 1995.
- Ian T Jolliffe, Nickolay T Trendafilov, and Mudassir Uddin. A modified principal component technique based on the LASSO. *Journal of Computational and Graphical Statistics*, 12(3):531–547, 2003.
- Michel Journée, Yurii Nesterov, Peter Richtárik, and Rodolphe Sepulchre. Generalized power method for sparse principal component analysis. *Journal of Machine Learning Research*, 11:517–553, 2010.
- Henry F Kaiser. The varimax criterion for analytic rotation in factor analysis. *Psychometrika*, 23(3):187–200, 1958.
- Henry F Kaiser. The application of electronic computers to factor analysis. *Educational and Psychological Measurement*, 20(1):141–151, 1960.
- Honglak Lee, Alexis Battle, Rajat Raina, and Andrew Y Ng. Efficient sparse coding algorithms. In *Proceedings of the 19th International Conference on Neural Information Processing Systems, NIPS’06*, page 801–808, Cambridge, MA, USA, 2006. MIT Press.
- Tianxi Li, Elizaveta Levina, and Ji Zhu. Network cross-validation by edge sampling. *Biometrika*, 107(2):257–276, 2020.
- Lester Mackey. Deflation methods for sparse PCA. In *Proceedings of the 21st International Conference on Neural Information Processing Systems, NIPS’08*, page 1017–1024, Red Hook, NY, USA, 2008. Curran Associates Inc.
- Kanti V Mardia. Measures of multivariate skewness and kurtosis with applications. *Biometrika*, 57(3):519–530, 1970.
- Jari Miettinen, Sara Taskinen, Klaus Nordhausen, and Hannu Oja. Fourth moments and independent component analysis. *Statistical Science*, 30(3):372–390, 2015.
- Baback Moghaddam, Yair Weiss, and Shai Avidan. Generalized spectral bounds for sparse LDA. In *Proceedings of the 23rd International Conference on Machine Learning, ICML’06*, page 641–648, New York, NY, USA, 2006. Association for Computing Machinery.

- Daniel T Montoro, Adam L Haber, Moshe Biton, Vladimir Vinarsky, Brian Lin, Susan E Birket, Feng Yuan, Sijia Chen, Hui Min Leung, Jorge Villoria, et al. A revised airway epithelial hierarchy includes CFTR-expressing ionocytes. *Nature*, 560(7718):319–324, 2018.
- Jorge Nocedal and Stephen Wright. *Numerical Optimization*. Springer Science & Business Media, New York, NY, USA, second edition, 2006.
- Bruno A Olshausen and David J Field. Emergence of simple-cell receptive field properties by learning a sparse code for natural images. *Nature*, 381(6583):607, 1996.
- Karl Pearson. On lines and planes of closest fit to systems of points in space. *The London, Edinburgh, and Dublin Philosophical Magazine and Journal of Science*, 2(11):559–572, 1901.
- Lindsey W Plasschaert, Rapolas Žilionis, Rayman Choo-Wing, Virginia Savova, Judith Knehr, Guglielmo Roma, Allon M Klein, and Aron B Jaffe. A single-cell atlas of the airway epithelium reveals the CFTR-rich pulmonary ionocyte. *Nature*, 560(7718):377–381, 2018.
- Karl Rohe and Muzhe Zeng. Vintage factor analysis with varimax performs statistical inference, 2020. arXiv:2004.05387.
- Karl Rohe, Tai Qin, and Bin Yu. Co-clustering directed graphs to discover asymmetries and directional communities. *Proceedings of the National Academy of Sciences*, 113(45):12679–12684, 2016.
- Richard J Samworth and Ming Yuan. Independent component analysis via nonparametric maximum likelihood estimation. *The Annals of Statistics*, 40(6):2973–3002, 2012.
- Dan Shen, Haipeng Shen, and James Stephen Marron. Consistency of sparse PCA in high dimension, low sample size contexts. *Journal of Multivariate Analysis*, 115:317–333, 2013.
- Haipeng Shen and Jianhua Z Huang. Sparse principal component analysis via regularized low rank matrix approximation. *Journal of Multivariate Analysis*, 99(6):1015–1034, 2008.
- Louis Leon Thurstone. Multiple factor analysis. *Psychological Review*, 38(5):406, 1931.
- Robert Tibshirani. Regression shrinkage and selection via the lasso. *Journal of the Royal Statistical Society. Series B (Methodological)*, pages 267–288, 1996.
- Andreas M Tillmann and Marc E Pfetsch. The computational complexity of the restricted isometry property, the nullspace property, and related concepts in compressed sensing. *IEEE Transactions on Information Theory*, 60(2):1248–1259, 2014.

- Olga Troyanskaya, Michael Cantor, Gavin Sherlock, Pat Brown, Trevor Hastie, Robert Tibshirani, David Botstein, and Russ B Altman. Missing value estimation methods for DNA microarrays. *Bioinformatics*, 17(6):520–525, 2001.
- Vincent Q Vu and Jing Lei. Minimax sparse principal subspace estimation in high dimensions. *The Annals of Statistics*, 41(6):2905–2947, 2013.
- Vincent Q Vu, Juhee Cho, Jing Lei, and Karl Rohe. Fantope projection and selection: A near-optimal convex relaxation of sparse PCA. In *Proceedings of the 26th International Conference on Neural Information Processing Systems*, NIPS’13, page 2670–2678, Red Hook, NY, USA, 2013. Curran Associates Inc.
- Tengyao Wang, Quentin Berthet, and Richard J Samworth. Statistical and computational trade-offs in estimation of sparse principal components. *The Annals of Statistics*, 44(5):1896–1930, 2016.
- Daniela M Witten, Robert Tibshirani, and Trevor Hastie. A penalized matrix decomposition, with applications to sparse principal components and canonical correlation analysis. *Biostatistics*, 10(3):515–534, 2009.
- Svante Wold. Cross-validatory estimation of the number of components in factor and principal components models. *Technometrics*, 20(4):397–405, 1978.
- Xiao-Tong Yuan and Tong Zhang. Truncated power method for sparse eigenvalue problems. *Journal of Machine Learning Research*, 14(1):899–925, 2013.
- Yilin Zhang and Karl Rohe. Understanding regularized spectral clustering via graph conductance. In *Proceedings of the 32nd International Conference on Neural Information Processing Systems*, NIPS’18, page 10654–10663, Red Hook, NY, USA, 2018. Curran Associates Inc.
- Yini Zhang, Fan Chen, and Karl Rohe. Social media public opinion as flocks in a murmuration. In preparation, 2021.
- Hui Zou and Trevor Hastie. Regularization and variable selection via the elastic net. *Journal of the Royal Statistical Society: Series B (Statistical Methodology)*, 67(2):301–320, 2005.
- Hui Zou and Lingzhou Xue. A selective overview of sparse principal component analysis. *Proceedings of the IEEE*, 106(8):1311–1320, 2018.
- Hui Zou, Trevor Hastie, and Robert Tibshirani. Sparse principal component analysis. *Journal of Computational and Graphical Statistics*, 15(2):265–286, 2006.